Off-shell behavior of nucleon self-energy in asymmetric nuclear matter

E. N. E. van Dalen[*] and H. Müther

Institut für Theoretische Physik, Universität Tübingen, Auf der Morgenstelle 14, D-72076 Tübingen, Germany

(Received 9 April 2010; published 29 July 2010)

The off-shell behavior of the nucleon self-energy in isospin-asymmetric nuclear matter is investigated within the framework of the relativistic Dirac-Brueckner-Hartree-Fock approach based on projection techniques. The dependence of the Dirac components of the self-energy on momentum as well as energy is evaluated for symmetric as well as asymmetric nuclear matter. Special attention is paid to the various contributions to the momentum dependence of the real and imaginary part of the optical potential. The consequences to the different definitions of the effective nucleon mass and particle spectral functions are discussed.

I. INTRODUCTION

The investigation of isospin-asymmetric nuclear matter is receiving a lot of attention because the exploration of nuclear systems outside the valley of stable nuclei are of high interest for astrophysical and nuclear-structure studies. In the field of astrophysics, these investigations are important for the physics of supernova explosions [1] and neutron stars [2–4], whereas in the field of nuclear structure they are of interest in the study of neutron-rich nuclei [5,6]. The new generation of radioactive-beam facilities, for example, the future GSI facility FAIR in Germany or SPIRAL2 at GANIL in France, facilitates this kind of nuclear-structure studies. Off-shell effects are crucial to describe the data obtained from the collisions occurring in these radioactive-beam experiments.

The theoretical models that are used to make predictions on the equation of state (EoS) of nuclear matter can roughly be divided in the following three classes: phenomenological density functionals, effective field theory (EFT) approaches, and *ab initio* approaches. Phenomenological density functionals are based on effective density-dependent interactions with usually between six and fifteen parameters. The EFT approaches lead to a more systematic expansion of the EoS in powers of the Fermi momentum k_F, respectively the density, with a small number of free parameters. The parameters of these models are typically adjusted to reproduce the properties of normal nuclei. Therefore, extrapolations outside the valley of stable nuclei must be considered with some scepticism.

Ab initio approaches, such as the Brueckner-Hartree-Fock (BHF) and the Dirac-Brueckner-Hartree-Fock (DBHF) approaches, are based on high-precision free-space nucleon-nucleon interactions and the nuclear many-body problem is treated microscopically. These approaches are more ambitious, because the predictions for the nuclear EoS are essentially parameter free. Therefore, they also have a higher predictive power for exotic nuclear systems.

Although nonrelativistic *ab initio* calculations were able to describe the nuclear saturation mechanism qualitatively, they failed quantitatively. Three-body forces were included in these nonrelativistic microscopic calculations to fit the empirical saturation point of symmetric nuclear matter as well as the properties of light nuclei. A major breakthrough was achieved when the first relativistic DBHF calculations were performed [7–9]. They could describe the saturation properties of nuclear matter without any need to introduce a three-nucleon force. In fact, it has been argued that the three-nucleon forces required in nonrelativistic calculations have to be introduced to simulate the change of the Dirac spinors in the nuclear medium, which is contained in relativistic calculations [10].

Beside this success of predicting the empirical saturation point, also the strength of the spin-orbit term in the single-particle spectrum of finite nuclei and the momentum dependence of the optical potential for nucleon-nucleus scattering [11,12] were considered as fingerprints of relativistic effects in nuclear-structure physics at low energies.

However, relativistic microscopic DBHF investigations of isospin-asymmetric nuclear matter are rather rare [13–17]. Furthermore, all these studies are restricted to the on-shell behavior of nucleon properties in contrast to some microscopic nonrelativistic investigations, which do include the study of off-shell behavior of these properties in isospin-asymmetric nuclear matter [18,19]. Only in isospin-symmetric nuclear matter is some attention paid to off-shell behavior in the framework of relativistic microscopic studies [21,22]. This means that in microscopic relativistic frameworks, the off-shell behavior of nucleon properties in isospin-asymmetric nuclear matter has not been investigated so far.

In this work, we describe the off-shell behavior of nucleon properties in isospin-asymmetric nuclear matter in the relativistic DBHF approach using the Bonn A potential and its bare NN matrix elements V [23]. Furthermore, the optimal representation scheme for the T matrix, the subtracted T-matrix representation, is applied. In this framework, the dependence of the off-shell behavior of nucleon properties on the nuclear asymmetry is explored. Properties considered are the optical potential, spectral functions, single-particle energies, and masses. Our predictions are compared to those of nonrelativistic calculations. Quantities of special interest are the k-mass and the E-mass, because a rigorous distinction between these two masses can only be obtained from the knowledge of the off-shell behavior of the optical potential.

The plan of this article is as follows. The relativistic DBHF approach is discussed in Sec. II. Furthermore,

───────
[*]eric.van-dalen@uni-tuebingen.de

Sec. III is devoted to the covariant representation of the in-medium T matrix in connection with the nucleon self-energy components depending on energy and momentum. The results are presented and discussed in Sec. IV. Finally, we end with a summary and a conclusion in Sec. V.

II. DBHF APPROACH

In this section, the relativistic Brueckner approach is discussed. The approach is roughly based on the ones in Refs. [16,17], with the exception of some modifications to separate the momentum and energy dependence. First, a general overview is given, followed by a discussion of the modifications.

In the relativistic Brueckner approach, the in-medium interaction of the nucleons is treated in the ladder approximation of the relativistic Bethe-Salpeter (BS) equation:

$$T = V + i \int V Q G G T, \tag{1}$$

where T denotes the T matrix, V is the bare nucleon-nucleon interaction, and Q is the Pauli operator. The Green's function G describes the propagation of dressed nucleons in nuclear matter. Furthermore, it fulfills the Dyson equation:

$$G = G_0 + G_0 \Sigma G, \tag{2}$$

where G_0 is the free nucleon propagator. The self-energy Σ in the Hartree-Fock (HF) approximation is given by

$$\Sigma = -i \int_F (Tr[GT] - GT). \tag{3}$$

The coupled set of Eqs. (1)–(3) presents a self-consistency problem and has to be iterated until convergence is reached.

To solve the self-consistency problem, some approximations have to be made in the iteration procedure. The first one is the quasiparticle approximation; that is, the imaginary part of the self-energy ImΣ is neglected. In addition, the "reference spectrum approximation" [24] is applied; that is, the effective mass of the nucleon is assumed to be entirely density dependent ($k = |\mathbf{k}| = k_F$). Furthermore, the two-particle propagator iGG in the BS equation is replaced by the Thompson propagator to reduce the four-dimensional BS integral equation, Eq. (1), to the three-dimensional Thompson equation. After a partial wave projection onto the $|JMLS\rangle$ states, this Thomas equation reduces to a set of one-dimensional integral equations over the relative momentum. To achieve this reduction to the one-dimensional integral equations, the Pauli operator Q is replaced by an angle-averaged Pauli operator $\overline{Q}$ [8]. For more details, we refer to [16,17].

At the end of the iteration procedure, we keep the explicit momentum and energy dependence in contrast to Refs. [16,17], in which the starting energy is replaced by its on-shell value. In this way, one obtains the nucleon self-energy

$$\Sigma(k, \omega) = \Sigma_s(k, \omega) - \gamma_0 \Sigma_o(k, \omega) + \boldsymbol{\gamma} \cdot \mathbf{k} \Sigma_v(k, \omega), \tag{4}$$

as a function of the absolute momentum $k = |\mathbf{k}|$ and energy ω. Apart from a real part, these self-energy components contain an imaginary part, which also can be calculated at the end of

the iteration procedure. These components of the self-energy are easily determined by taking the respective traces [8,25]

$$\Sigma_s = \frac{1}{4} \text{tr}[\Sigma], \quad \Sigma_o = \frac{-1}{4} \text{tr}[\gamma_0 \, \Sigma], \quad \Sigma_v = \frac{-1}{4|\mathbf{k}|^2} \text{tr}[\boldsymbol{\gamma} \cdot \mathbf{k} \, \Sigma]. \tag{5}$$

The other quantities, such as the effective Dirac mass, single-particle energy, and the optical potential, can be obtained from these self-energy components.

III. COVARIANT REPRESENTATION AND THE SELF-ENERGY COMPONENTS

Because the T-matrix elements are determined in the two-particle c.m. frame, a representation with covariant operators and Lorentz invariant amplitudes in Dirac space is the most convenient way to Lorentz transform the positive-energy-projected T matrix from the two-particle c.m. frame into the nuclear-matter rest frame [8]. The restriction to positive-energy states causes ambiguities, because pseudoscalar (ps) and pseudovector (pv) components cannot uniquely be disentangled in on-shell scattering. Therefore, some freedom in the choice of this representation exists. The different choices of representations such as the ps representation and the complete pv representation are elaborately discussed in Refs. [16,17,26]. Only the complete pv representation succeeds in reproducing the HF nucleon self-energy, applying pv mesons such as the π and η meson as bare interaction. However, this complete pv representation fails to reproduce the HF nucleon self-energy if meson exchange potentials are applied other than that of pv mesons. In contrast, the ps representation reproduces the HF self-energy for these other mesons. Because the influence of the pv mesons, in particular that of the π meson, is dominantly given by the single-meson exchange, this ambiguity can be minimized by separating the single-π and -η exchange from the full T matrix. The contributions stemming from the single-π and -η exchange are then given in the complete pv representation, whereas for the remaining part of the T matrix,

$$T_{\text{Sub}} = T - V_{\pi,\eta}, \tag{6}$$

the ps representation is chosen. In this case, the final nuclear-matter bulk properties depend only moderately on the representation scheme, as discussed in Ref. [26]. This representation scheme, using the ps representation as well as the complete pv representation, is the optimal representation scheme so far and is called the subtracted-T-matrix representation scheme [16,17,26].

For the ps representation, the following set of five linearly independent covariants,

$$\text{S} = 1_1 \otimes 1_2, \tag{7}$$

$$\text{V} = (\gamma^\mu)_1 \otimes (\gamma_\mu)_2, \tag{8}$$

$$\text{T} = (\sigma^{\mu\nu})_1 \otimes (\sigma_{\mu\nu})_2, \tag{9}$$

$$\text{A} = (\gamma_5)_1(\gamma^\mu)_1 \otimes (\gamma_5)_2(\gamma_\mu)_2, \tag{10}$$

$$\text{P} = (\gamma_5)_1 \otimes (\gamma_5)_2, \tag{11}$$

are used in isospin-symmetric nuclear matter. The interchanged invariants are defined as [27] $\tilde{\text{S}} = \tilde{\text{S}}\text{S}$, $\tilde{\text{V}} = \tilde{\text{S}}\text{V}$,

$\tilde{T} = \tilde{S}T$, $\tilde{A} = \tilde{S}A$, and $\tilde{P} = \tilde{S}P$ with operator $\tilde{S}$ exchanging particles 1 and 2, that is, $\tilde{S}u(1)_\sigma u(2)_\tau = u(1)_\tau u(2)_\sigma$. In isospin-asymmetric nuclear, one needs an additional covariant for the np channel. It is defined as

$$I = 1_1 \otimes (\gamma \cdot k)_2 + (\gamma \cdot k)_1 \otimes 1_2. \tag{12}$$

Taking the single nucleon momentum $\mathbf{k} = (0, 0, |\mathbf{k}|)$ along the z axis, then we have for the self-energy components in the ps representation scheme

$$\Sigma_s^{ij}(|\mathbf{k}|, \omega) = \frac{1}{4} \int_0^{k_{Fj}} \frac{d^3\mathbf{q}}{(2\pi)^3} \frac{m_j^*}{E_{q,j}^*} \left[4F_S^{ij} - F_{\tilde{S}}^{ij} - 4F_{\tilde{V}}^{ij} - 12F_{\tilde{T}}^{ij} \right.$$
$$\left. + 4F_{\tilde{A}}^{ij} - F_{\tilde{P}}^{ij} + 4(1 - \delta_{ij}) \frac{k^{*\mu}q_\mu^* - m_j^{*2}}{m_j^*} F_I^{ij} \right], \tag{13}$$

$$\Sigma_o^{ij}(|\mathbf{k}|, \omega) = \frac{1}{4} \int_0^{k_{Fj}} \frac{d^3\mathbf{q}}{(2\pi)^3} \left[-4F_V^{ij} + F_{\tilde{S}}^{ij} - 2F_{\tilde{V}}^{ij} - 2F_{\tilde{A}}^{ij} \right.$$
$$\left. - F_{\tilde{P}}^{ij} + 4(1 - \delta_{ij})m_j^* \frac{E_{k,i}^* - E_{q,j}^*}{E_{q,j}^*} F_I^{ij} \right], \tag{14}$$

and

$$\Sigma_v^{ij}(|\mathbf{k}|, \omega) = \frac{1}{4} \int_0^{k_{Fj}} \frac{d^3\mathbf{q}}{(2\pi)^3} \frac{\mathbf{q} \cdot \mathbf{k}}{|\mathbf{k}|^2 E_{q,j}^*} \left[-4F_V^{ij} + F_{\tilde{S}}^{ij} - 2F_{\tilde{V}}^{ij} \right.$$
$$\left. - 2F_{\tilde{A}}^{ij} - F_{\tilde{P}}^{ij} - 4(1 - \delta_{ij})m_j^* \frac{|\mathbf{k}| - q_z}{q_z} F_I^{ij} \right], \tag{15}$$

where $k_i^{*\mu} = (E_{k,i}^*, 0, 0, |\mathbf{k}|)$. A relation exists between our definition of the energy ω and $E_{k,i}^* = \omega + \Sigma_o^i(|\mathbf{k}|, \omega) + M$. Furthermore, the Lorentz invariant amplitudes F have a dependence on the absolute momentum $|\mathbf{k}|$ as well as the energy ω.

In the complete pv representation applied to the contributions stemming from the single-π and -η exchange, one first applies the identities

$$\tfrac{1}{2}(T + \tilde{T}) = S + \tilde{S} + P + \tilde{P}, \tag{16}$$
$$V + \tilde{V} = S + \tilde{S} - P - \tilde{P}, \tag{17}$$

to replace tensor and vector covariants. Next, the ps covariant $P = (\gamma_5)_1 \otimes (\gamma_5)_2$ in the T-matrix representation is replaced by the pv covariant,

$$PV = \frac{(\gamma_5\gamma_\mu)_1 p^\mu}{m_i^* + m_j^*} \otimes \frac{(\gamma_5\gamma_\mu)_2 p^\mu}{m_i^* + m_j^*}, \tag{18}$$

with $p^\mu = k^\mu - q^\mu$. The contributions to the self-energy components are then given by

$$\Sigma_s^{ij}(|\mathbf{k}|, \omega) = \frac{1}{4} \int_0^{k_{Fj}} \frac{d^3\mathbf{q}}{(2\pi)^3} \frac{m_j^*}{E_{q,j}^*} \left[4g_S^{ij} - g_{\tilde{S}}^{ij} + 4g_A^{ij} \right.$$
$$+ \frac{m_j^{*2} + m_i^{*2} - 2k^{*\mu}q_\mu^*}{(m_i^* + m_j^*)^2} g_{\widetilde{PV}}^{ij}$$
$$\left. + 4(1 - \delta_{ij}) \frac{k^{*\mu}q_\mu^* - m_j^{*2}}{m_j^*} g_I^{ij} \right], \tag{19}$$

$$\Sigma_o^{ij}(|\mathbf{k}|, \omega) = +\frac{1}{4} \int_0^{k_{Fj}} \frac{d^3\mathbf{q}}{(2\pi)^3} \left[g_{\tilde{S}}^{ij} - 2g_A^{ij} \right.$$
$$- \frac{2E_{k,i}^*\left(m_j^{*2} - k^{*\mu}q_\mu^*\right) - E_{q,j}^*\left(m_j^{*2} - m_i^{*2}\right)}{E_{q,j}^*\left(m_i^* + m_j^*\right)^2} g_{\widetilde{PV}}^{ij}$$
$$\left. + 4(1 - \delta_{ij})m_j^* \frac{E_{k,i}^* - E_{q,j}^*}{E_{q,j}^*} g_I^{ij} \right], \tag{20}$$

and

$$\Sigma_v^{ij}(|\mathbf{k}|, \omega) = \frac{1}{4} \int_0^{k_{Fj}} \frac{d^3\mathbf{q}}{(2\pi)^3} \frac{\mathbf{q} \cdot \mathbf{k}}{|\mathbf{k}|^2 E_{q,j}^*} \left[g_{\tilde{S}}^{ij} - 2g_A^{ij} \right.$$
$$- \frac{2k_z^*\left(m_j^{*2} - k^{*\mu}q_\mu^*\right) - q_z\left(m_j^{*2} - m_i^{*2}\right)}{q_z\left(m_i^* + m_j^*\right)^2} g_{\widetilde{PV}}^{ij}$$
$$\left. - 4(1 - \delta_{ij})m_j^* \frac{|\mathbf{k}| - q_z}{q_z} g_I^{ij} \right], \tag{21}$$

where the new amplitudes g are defined as

$$\begin{pmatrix} g_S^{ij} \\ g_{\tilde{S}}^{ij} \\ g_A^{ij} \\ g_{PV}^{ij} \\ g_{\widetilde{PV}}^{ij} \end{pmatrix} = \frac{1}{4} \begin{pmatrix} 4 & -2 & -8 & 0 & -2 \\ 0 & -6 & -16 & 0 & 2 \\ 0 & -2 & 0 & 0 & -2 \\ 0 & 2 & -8 & 4 & 2 \\ 0 & 6 & -16 & 0 & -2 \end{pmatrix} \begin{pmatrix} F_S^{ij} \\ F_V^{ij} \\ F_T^{ij} \\ F_P^{ij} \\ F_A^{ij} \end{pmatrix} \tag{22}$$

and $g_I^{ij} = F_I^{ij}$.

Finally, the total neutron and proton self-energies including all channels can be written as

$$\Sigma^n(|\mathbf{k}|, \omega) = \Sigma^{nn}(|\mathbf{k}|, \omega) + \Sigma^{np}(|\mathbf{k}|, \omega);$$
$$\Sigma^p(|\mathbf{k}|, \omega) = \Sigma^{pp}(|\mathbf{k}|, \omega) + \Sigma^{pn}(\mathbf{k}, \omega), \tag{23}$$

respectively.

IV. RESULTS

In the following, we present the results for the off-shell properties of isospin-symmetric and asymmetric nuclear matter obtained from the DBHF approach based on projection techniques. The applied projection is the subtracted T-matrix representation scheme. Furthermore, the nucleon-nucleon potential used is Bonn A. The presented results are obtained from calculations performed at a density of $n_B = 0.181$ fm^{-3} in isospin-symmetric nuclear matter and with the asymmetry parameter of $\beta = (n_n - n_p)/n_B = 0.5$ in isospin-asymmetric nuclear matter.

A. Self-energy

The energy and momentum dependencies of the imaginary part of the self-energy components at the saturation density of our EoS in isospin-symmetric nuclear matter are depicted in Fig. 1.
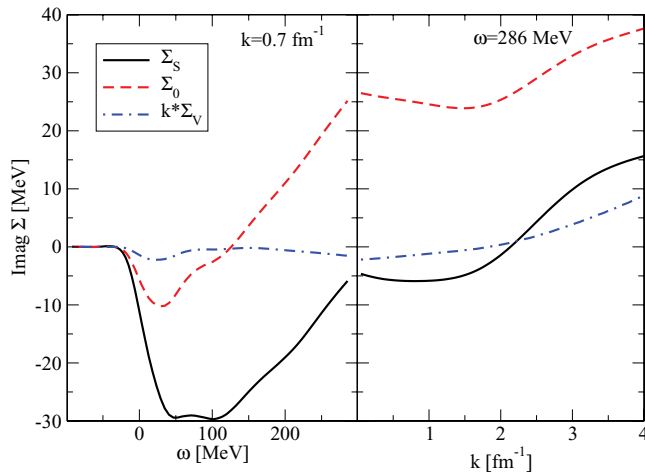
FIG. 1. (Color online) The imaginary part of the self-energy components calculated in isospin-symmetric nuclear matter at a density of $n_B = 0.181$ fm^{-3}. Left: energy dependence; right: momentum dependence.

Because only particle-particle ladders are included in the solution of the BS equation (1), which defines the T matrix, these imaginary self-energy components are different from zero for energies above the Fermi energy of -26.5 MeV. For energies just above this threshold, the imaginary part of the scalar component Σ_s as well as of the timelike vector component Σ_0 are negative, which implies that they tend to compensate each other in the Dirac equation for the upper component. At larger values for the energy ω, the difference $\Sigma_s - \Sigma_0$ essentially remains constant. This is very different from results obtained within a simple $\sigma\omega$ model [28], indicating that the iterated π exchange terms are dominating the two-particle–one-hole contributions to the self-energy when a realistic interaction model is used. The imaginary part of the spacelike vector component Σ_v is rather small.

An example for energy and momentum dependence of the real part of the nucleon self-energy is shown in Fig. 2.
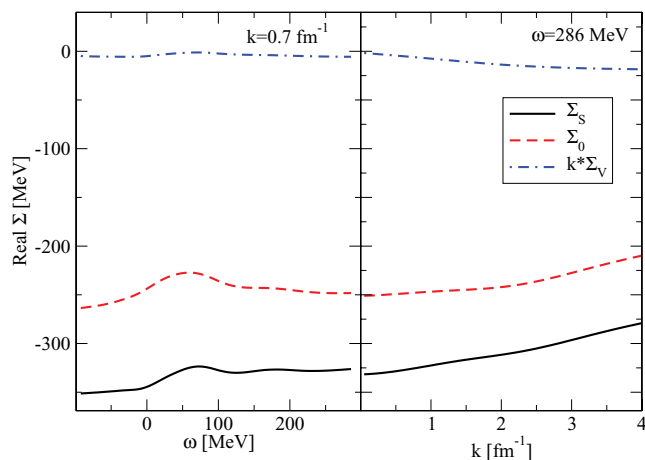

FIG. 2. (Color online) The real part of the self-energy components calculated in isospin-symmetric nuclear matter at density of $n_B = 0.181$ fm^{-3}. Left: energy dependence; right: momentum dependence.

In the energy dependence, a small enhancement appears just above the Fermi energy of -26.5 MeV, where the imaginary self-energy components turn nonzero. However, the energy dependence of the real part of nucleon self-energy is still rather weak. The moment dependence shows a very smooth behavior. The degree of sensitivity of the self-energy components on energy ω and momentum k shown in Fig. 2 is relevant for the "reference spectrum approximation" used in the iteration procedure, because strong momentum and energy dependencies question the validity of the reference spectrum approximation. However, the energy and momentum dependencies of the self-energy components can be characterized as rather weak, as can be seen in Fig. 2. One must keep in mind, however, that Fig. 2 shows two quantities, Σ_s and Σ_0, which are big and compensate for each other to a large extent when inserted into the Dirac equation. Therefore, a weak dependence of these components can get magnified in solving the Dirac equation. Therefore, in the following, we use these momentum- and energy-dependent components but discuss combinations of these components that are relevant for nuclear physics at low energies.

B. Optical potentials and spectral functions

An interesting quantity is the Schrödinger equivalent optical potential. This potential is obtained when the Dirac equation is reduced to an equivalent Schrödinger equation for the large component of the Dirac spinor. Therefore, it can be identified with the nonrelativistic optical potential for a nucleon inside the nuclear medium. This potential,

$$U(|\mathbf{k}|, \omega) = \Sigma_s(|\mathbf{k}|, \omega) - \frac{1}{M} k^\mu \Sigma_\mu(|\mathbf{k}|, \omega)$$
$$+ \frac{\Sigma_s^2(|\mathbf{k}|, \omega) - \Sigma_\mu^2(|\mathbf{k}|, \omega)}{2M}, \qquad (24)$$

can be obtained from the relativistic self-energy components in Eq. (4). Of special interest is the on-shell value of this optical potential, which means that we consider the case $\omega = \varepsilon(|\mathbf{k}|)$ with the single-particle energy defined in (27). Results for the real part of this optical potential are displayed in Fig. 3 (solid line).

What determines the momentum dependence of this optical potential? If one ignores the energy and momentum dependencies of relativistic self-energy components using, for example ($k = |\mathbf{k}| = k_F$ and $\omega = \varepsilon_F$, one obtains a momentum dependence as presented by the dash-dotted line in Fig. 3. This momentum dependence is a relativistic feature because it originates from the reduction of the Dirac equation to the nonrelativistic Schrödinger equation. That is why we have labeled this curve as the Dirac dependence.

If in a next step the momentum dependence of the relativistic components of the self-energy is taken into account (keeping $\omega = \varepsilon_F$), the dashed line is obtained. We see that the inclusion of this nonlocality in space, which mainly originates from the Fock exchange term in the self-energy, tends to enhance the momentum dependence of the optical potential (see dashed line, labeled "Dirac and momentum dependence").

The effects of the momentum dependence are partly compensated if the energy dependence of the self-energy is
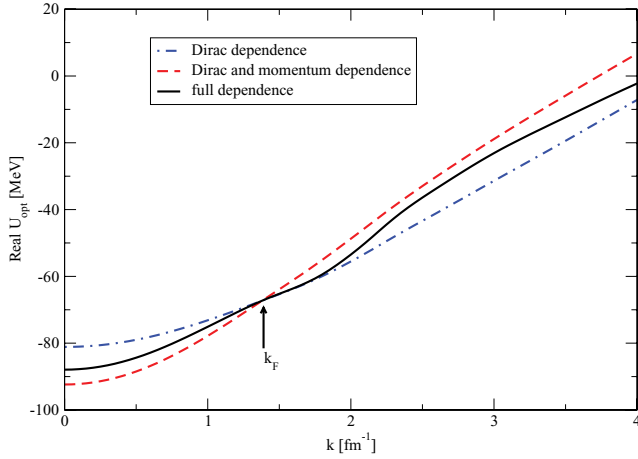
FIG. 3. (Color online) The real part of the on-shell optical potential as defined in Eq. (24) for $\omega = \varepsilon(|\mathbf{k}|)$ for symmetric nuclear matter at fixed nuclear density $n_B = 0.181$ fm^{-3}. The various approximations are discussed in the text.

also considered. The full result is rather close to the Dirac-only approach, in particular close to the Fermi surface.

The energy dependencies of the neutron and proton optical potentials in isospin-asymmetric nuclear matter with an asymmetry parameter of $\beta = 0.5$ are plotted in Fig. 4 for various values of the momentum k.

The lower panels show the corresponding imaginary parts of these potentials. These imaginary parts are identical to zero for energies ω less than the corresponding Fermi energy, that is, $\omega < \varepsilon_F$. At energies just above the Fermi energy, they initially decrease with a steep negative slope and then seem to stabilize. This stabilization is identical to the example of symmetric nuclear matter, as we discussed before in connection with Fig. 1. It should be recalled, however, that at smaller energy, the main contribution originates from the imaginary part of
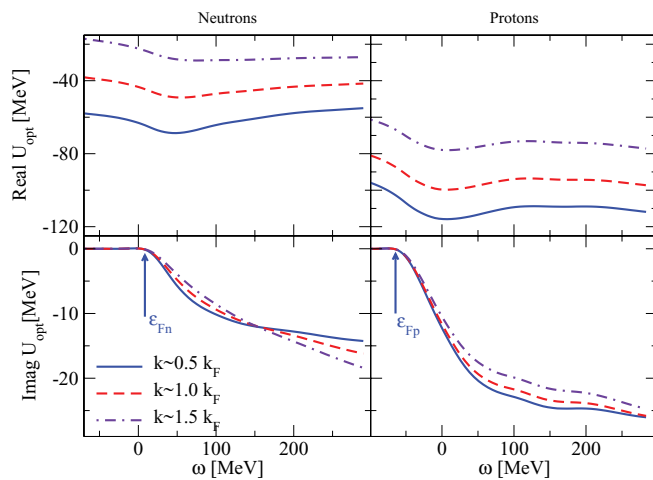

FIG. 4. (Color online) The energy dependence of the optical potential for neutrons (left panels) and protons (right panels) in isospin-asymmetric nuclear matter with an asymmetry parameter of $\beta = 0.5$ at fixed nuclear density $n_B = 0.181$ fm^{-3}. The real part (upper panels) and the imaginary part (lower panels) of the nucleon optical potential are plotted for various momenta.

Σ_s, whereas at energies $\omega > 200$ MeV, the vector component Σ_0 tends to dominate. The momentum dependence of the imaginary part is rather weak.

The real part of the optical potential gets more attractive with increasing energy until one reaches values of the energy at which the imaginary part is different from zero. The real part then turns less attractive at higher energies. Therefore, the energy dependence of the real part of the optical potential displays a minimum at energies just above the Fermi energies, as can be seen in the upper panels of Fig. 4. Such a minimum around the Fermi energy is also found in the self-energy from nonrelativistic BHF calculations [29]. Another observation made from Fig. 4 concerns the momentum dependence. It is found that the real part of optical potential becomes less attractive with increasing momenta.

In isospin-asymmetric nuclear matter, the properties of neutrons and protons differ from each other, as one can see by comparing the panels on the left and right sides of Fig. 4. The real part of the proton optical potential is more attractive than that of the neutron optical potential in neutron-rich matter. Also, the absolute values for the imaginary part are larger for protons than for the neutrons. These results are easy to understand because the proton-neutron interaction is stronger than the neutron-neutron or proton-proton interactions. Therefore, the protons are exposed to a stronger mean field, which is caused mainly by the interaction with the large number of neutrons around.

The real and imaginary parts of the optical potential can also be used to determine the spectral function for the particle strength from its nonrelativistic definition,

$$S^p(|\mathbf{k}|, \omega)$$
$$= -\frac{1}{\pi} \frac{\text{Im}U(|\mathbf{k}|, \omega)}{[\omega - k^2/2M - \text{Re}U(|\mathbf{k}|, \omega)]^2 + [\text{Im}U(|\mathbf{k}|, \omega)]^2},$$
$$(25)$$

for $\omega > \varepsilon_F$. It represents the probability that a nucleon with momentum $k = |\mathbf{k}|$ and energy ω can be added to the ground state. Figure 5 displays the spectral functions for protons and neutrons in isospin-asymmetric nuclear matter with an asymmetry parameter of $\beta = 0.5$ at fixed nuclear density of $n_B = 0.181$ fm^{-3}.

The upper part of this figure shows the particle strength for momenta below the corresponding Fermi momenta for protons and neutrons. In the independent-particle model, states with these momenta would be completely occupied and the particle strength is identical to zero. Because, however, the Brueckner G matrix accounts for particle-particle ladders, the BHF and also the DBHF self-energies include the effects of two-particle–one-hole terms, which lead to a nonvanishing imaginary part for $\omega > \varepsilon_F$. Because of these two-particle–one-hole components, we observe a nonvanishing spectral particle strength for momenta below k_F. From the upper part of Fig. 5, we can see that the larger values of the imaginary part of the proton optical potential displayed in Fig. 4 lead to larger values for the proton spectral functions than for the neutron spectral functions. This has also been observed in nonrelativistic calculations of asymmetric nuclear matter [19].
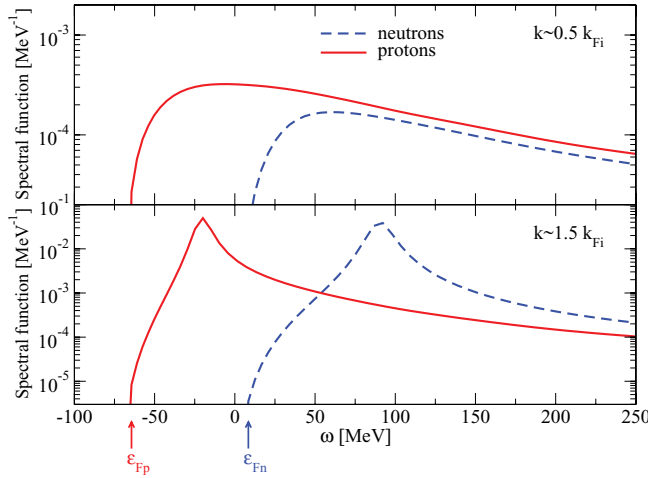
FIG. 5. (Color online) Particle spectral functions for nucleons with $k \sim 0.5\ k_{Fi}$ in the upper part and $k \sim 1.5\ k_{Fi}$ in the lower panel as a function of energy ω in isospin-asymmetric nuclear matter with an asymmetry parameter of $\beta = 0.5$ at fixed nuclear density of $n_B = 0.181$ fm^{-3}.

This nonvanishing particle strength for momenta below k_F should be accompanied by a depletion of the occupation number below 1 for these states. Note, however, that the BHF approach and the DBHF approximation are not number conserving. Because they do not account for hole-hole ladder terms, one does not obtain a spectral distribution for energies $\omega < \varepsilon_F$. The depletion of the occupation numbers for the hole states ($k < k_F$), however, can be determined from the single-particle strength at the quasiparticle poles of the single-particle Green's function [20]:

$$z(k = |\mathbf{k}|) = \left\{ 1 - \left(\frac{\partial \mathrm{Re} U(|\mathbf{k}|, \omega)}{\partial \omega} \right)_{\omega = \varepsilon(|\mathbf{k}|)} \right\}^{-1}. \quad (26)$$

Because the energy dependence of the real part of the optical potential in neutron-rich matter is larger for the protons than for the neutrons (see Fig. 4), we obtain larger depletions for the protons than for the neutrons. While the neutron occupation number varies between 0.95 for $k \approx 0.5 k_{Fn}$ and 0.87 for $k \approx k_{Fn}$, the corresponding numbers for the proton are 0.87 ($k \approx 0.5 k_{Fp}$) and 0.8 ($k \approx k_{Fp}$). The stronger proton-neutron interaction yields a larger depletion for the protons than for the neutrons in neutron-rich matter.

The lower panel of Fig. 5 shows the particle-strength distribution for momenta larger than the Fermi momentum. The imaginary part of the self-energy leads to a broad distribution of the single-particle strength.

C. Single-particle energy

The relativistic expression of the single-particle energy is given by

$$\varepsilon(|\mathbf{k}|, \omega) = -\Sigma_o(|\mathbf{k}|, \omega) + [1 + \Sigma_v(|\mathbf{k}|, \omega)]$$

$$\times \sqrt{\mathbf{k}^2 + \left(\frac{M + \Sigma_s(|\mathbf{k}|, \omega)}{1 + \Sigma_v(|\mathbf{k}|, \omega)} \right)^2} - M. \quad (27)$$
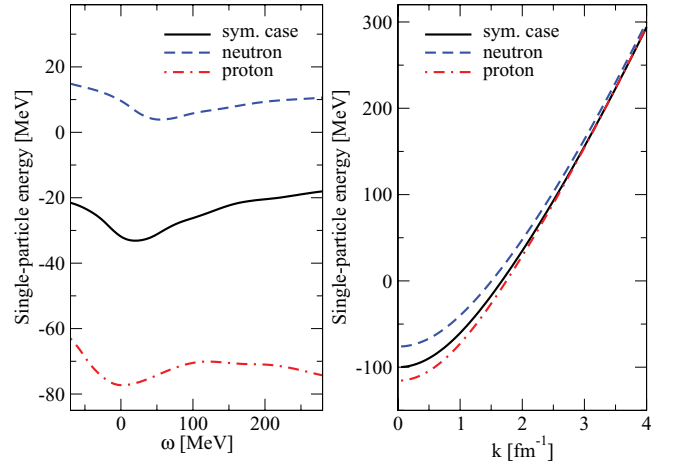

FIG. 6. (Color online) Energy and momentum dependence of the single-particle energy. The neutron (dashed line) and proton (dash-dotted line) single-particle energies are depicted for isospin-asymmetric nuclear matter with an asymmetry parameter of $\beta = 0.5$ at a fixed nuclear density of $n_B = 0.181$ fm^{-3}. The nucleon single-particle energy in isospin-symmetric nuclear matter (solid line) is also given. Left: energy dependence at $k = k_{Fi}$. Right: momentum dependence at $\omega = \varepsilon_{Fi}$.

Energy and momentum dependence of the single-particle energy in isospin-symmetric and -asymmetric nuclear are plotted in Fig. 6.

The energy dependence of the single-particle potential in the left panel displays a minimum at energies just above the Fermi energies, which is related to the small enhancement in the real part of the self-energy. In the right panel, a rough quadratic dependence of the single-particle energy on the momentum k is found. Such a quadratic dependence is often assumed in nonrelativistic calculations [29],

$$\varepsilon \approx \frac{k^2}{2M^*} + C. \quad (28)$$

Furthermore, in Fig. 6 the neutron has a higher single-particle energy than the proton because of its less attractive potential in neutron-rich matter.

D. Effective mass

A common concept in the field of nuclear physics is the effective mass. However, the expression of an effective nucleon mass has been used in various connections in many-body physics and to denote different quantities. This includes the nonrelativistic effective mass m_{NR}^* and the relativistic Dirac mass m_D^*.

The Dirac mass is a genuine relativistic quantity and can only be obtained from relativistic many-body approaches. The effective Dirac mass accounts for medium effects through the scalar part of the self-energy. It is given by

$$m_D^*(|\mathbf{k}|, \omega) = \frac{M + \mathrm{Re}\Sigma_s(|\mathbf{k}|, \omega)}{1 + \mathrm{Re}\Sigma_v(|\mathbf{k}|, \omega)}. \quad (29)$$

The energy and momentum dependency of this Dirac mass are plotted in Fig. 7.
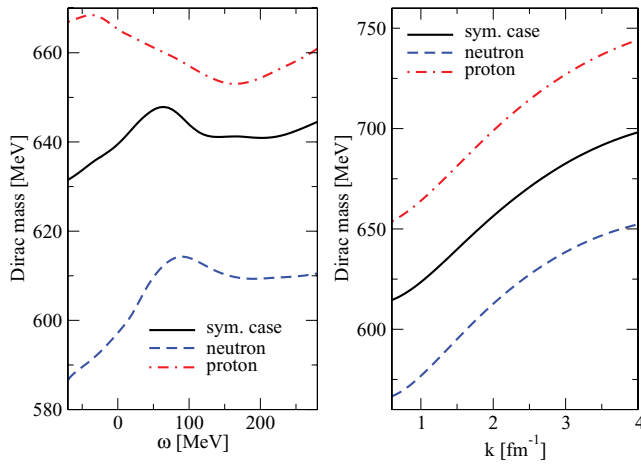
FIG. 7. (Color online) Energy and momentum dependence of the Dirac mass. The neutron (dashed line) and proton (dash-dotted line) Dirac masses are depicted for isospin-asymmetric nuclear matter with asymmetry parameter $\beta = 0.5$ at a fixed nuclear density of $n_B = 0.181$ fm^{-3}. The nucleon Dirac mass in isospin-symmetric nuclear matter (solid line) is also given. Left: energy dependence at $k = k_{Fi}$. Right: momentum dependence at $\omega = \varepsilon_{Fi}$.

FIG. 8. (Color online) The effective nonrelativistic mass (solid lines), the effective k-mass (dashed lines), and the effective E-mass (dash-dotted lines) at the on-shell point, that is, $\omega = \varepsilon(|\mathbf{k}|, \omega)$, for neutrons and protons as obtained from relativistic DBHF calculations for isospin-asymmetric nuclear matter at a density of $n_B = 0.181$ fm^{-3} and a proton abundance of 25 % ($\beta = 0.5$).

The maximum in the Dirac mass just above the Fermi energy in the left panel in Fig. 7 originates from the small enhancement in the scalar self-energy. In the right panel, the smooth behavior of the momentum dependence can be observed. In addition, it can be observed that the effective Dirac mass of the proton is larger than that of the neutron. This result of the larger proton Dirac mass in neutron-rich matter has been mentioned in previous DBHF calculations based on projection techniques [14,16,17,30–32].

In contrast, the nonrelativistic mass is the result of a quadratic parametrization of the single-particle spectrum mentioned in Sec. IV C [see Eq. (28)]. It is a measure of the nonlocality of the single-particle potential U. Therefore, the effective nonrelativistic mass is given by

$$m^*_{NR}[|\mathbf{k}|, \omega = \varepsilon(|\mathbf{k}|, \omega)]$$
$$= \left[\frac{1}{M} + \frac{1}{|\mathbf{k}|} \frac{\partial U[|\mathbf{k}|, \omega = \varepsilon(|\mathbf{k}|, \omega)]}{\partial |\mathbf{k}|}\right]^{-1}. \quad (30)$$

The nonlocality of U can be due to nonlocalities in space, which results in a momentum dependence, or in time, which results in an energy dependence. To separate both effects, these two types of nonlocalities have been characterized by the k-mass,

$$m^*_k(|\mathbf{k}|, \omega) = \left[\frac{1}{M} + \frac{1}{|\mathbf{k}|} \frac{\partial U(|\mathbf{k}|, \omega)}{\partial |\mathbf{k}|}\right]^{-1}, \quad (31)$$

and by the E-mass,

$$m^*_E(|\mathbf{k}|, \omega) = M \left[1 - \frac{\partial U(|\mathbf{k}|, \omega)}{\partial \omega}\right], \quad (32)$$

respectively. These masses can be determined from both, as well relativistic as nonrelativistic approaches.

In Fig. 8, the presented masses at the on-shell point, that is, $\omega = \varepsilon(|\mathbf{k}|, \omega)$, are obtained from our relativistic DBHF calculation using Eq. (24).
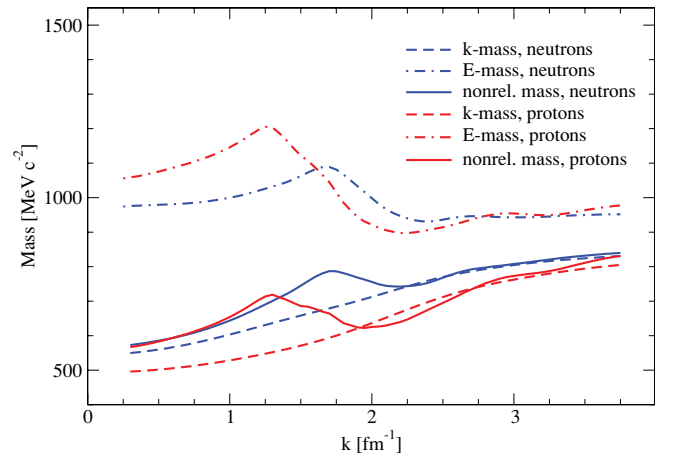
The pronounced peak of the nonrelativistic mass slightly above k_F, as is also seen in nonrelativistic Green's function calculations [33] and BHF calculations [19,34,35], is reproduced. This peak structure of the nonrelativistic mass is the result of subtle cancellation effects of the scalar and vector self-energy components in the relativistic framework. Therefore, a very precise method is required to determine variations of the self-energy, because they are small compared to their absolute scale. The applied projection techniques are the adequate tool for this purpose, whereas the extraction of mean self-energy components from a fit to the single-particle potential [15] is not able to resolve such a structure at all.

Another issue concerns isospin-asymmetric properties, that is, the proton-neutron mass splitting. Although the Dirac mass derived from the DBHF approach has a proton-neutron mass splitting of $m^*_{D,n} < m^*_{D,p}$ as can be seen from Fig. 7, the nonrelativistic mass derived from the DBHF approach shows the opposite behavior, that is, $m^*_{NR,n} > m^*_{NR,p}$, which is in agreement with the results from nonrelativistic BHF calculations [18,19]. This has been investigated earlier in the works of Refs. [31,32]. However, the k-mass and E-mass from these relativistic approaches are not considered in these works, because the determination of these two masses requires the knowledge of the off-shell behavior of the single-particle potential U.

These k-masses and E-masses obtained from our relativistic DBHF calculations are plotted in Fig. 8 for isospin-asymmetric nuclear matter at a density of $n_B = 0.181$ fm^{-3} and an asymmetry parameter of $\beta = 0.5$. The effective k-mass, which corresponds to the nonlocalities in space of single-particle potential, are mainly generated by exchange Fock terms. It can be observed that the resulting k-mass is a smooth function of the momentum, which is also in agreement with results from nonrelativistic calculations [29]. Another observation is that the effective k-mass for the protons is significantly below the corresponding value for the neutrons

at all momenta. This result also is in agreement with results obtained from nonrelativistic BHF calculations [19,35].

The effective E-mass represents the nonlocality in time. This nonlocality in time is generated by Brueckner ladder correlations due to the scattering to intermediate states, which are off-shell. These are mainly short-range correlations that generate a strong momentum dependence with a characteristic enhancement of the E-mass slightly above the Fermi surface, as can be observed in Fig. 8. The maximum value is even higher than the bare mass M. This peak structure is also observed in the case of nonrelativistic calculations [19,29,34–36]. Therefore, the enhancement of the nonrelativistic mass is due to the effective E-mass. Because the effective E-mass is not strong enough to compensate for the effects of the k-mass, the effective nonrelativistic mass for neutrons remains larger than the corresponding one for protons.

V. SUMMARY AND CONCLUSION

In this work, we describe the off-shell behavior of nucleon properties in isospin-asymmetric nuclear matter in the relativistic DBHF approach based on projection techniques using the Bonn A potential. In addition, the optimal representation scheme for the T matrix, the subtracted T-matrix representation, is applied. At the end of the iteration procedure, we keep not only the momentum dependence but also the explicit energy dependence of the relativistic components of the self-energy for our investigation of the off-shell behavior of nucleon properties in isospin-asymmetric nuclear matter. These off-shell effects are relevant for reactions occurring in radioactive beam experiments.

An issue considered is the off-shell behavior of the optical potential and the related spectral function. Because the BHF approximation does not account for hole-hole ladder terms, the imaginary part of the relativistic self-energy components are identical to zero for energies below the Fermi energy. As a consequence, also the imaginary part of the optical potential and spectral function are identical to zero in this energy range. However, these quantities yield non-negligible values above the Fermi energy. The real part of the optical potential yields nonzero values in the entire energy range considered and displays a minimum at energies just above the Fermi energies. Furthermore, the real and the imaginary parts of the proton optical potential are much stronger than those of the neutron optical potential in neutron-rich matter. This is due to the stronger proton-neutron as compared to the neutron-neutron and proton-proton interactions. These larger

values of the imaginary part of the proton optical potential also lead to larger values for the particle spectral functions of hole states and the corresponding depletions of the occupation numbers for the hole states. This behavior has also be observed in nonrelativistic BHF calculations [19].

Another issue is the behavior of the nonrelativistic mass, which can be determined from relativistic as well as nonrelativistic approaches. The pronounced peak of the on-shell nonrelativistic mass slightly above $k_{\rm F}$, which is typical for nonrelativistic calculations [19,34,35], is reproduced in our relativistic calculation. This nonrelativistic mass is a measure of the nonlocality in space and in time. Nonlocalities in space, which result in a momentum dependence, are characterized by the k-mass, whereas nonlocalities in time, which result in an energy dependence, are characterized by the E-mass. Therefore, even the determination of the on-shell values of these quantities require the knowledge of the off-shell behavior of the single-particle potential. The effective k-mass shows a smooth behavior, whereas the E-mass exhibits a large peak slightly above the Fermi surface. Therefore, the observed strong enhancement of the nonrelativistic mass is due to the behavior of the E-mass. These predictions of the k and E-masses are in agreement with results from nonrelativistic calculations [29].

An observation concerning the isospin effects of these quantities is that the effective k-mass for the protons is significantly below the corresponding value for the neutrons. Because the effective E-mass is not strong enough to compensate for the effects of the k-mass, the effective nonrelativistic mass for neutrons remains larger than the corresponding one for protons. This result for the nonrelativistic mass splitting, which is opposite to the Dirac mass splitting of $m_{D,n}^* < m_{D,p}^*$ [31,32], is in agreement with the results from nonrelativistic BHF calculations [18,19].

Therefore, in the framework of the relativistic DBHF approach, we are able to obtain results for the off-shell behavior of nucleon properties in isospin-symmetric as well as isospin-asymmetric nuclear matter. These results for the nucleon properties such as nucleon optical potentials, spectral functions, single-particle energies, and effective masses can be applied in the description of nucleon-nucleon collisions occurring in radioactive beam experiments.

[1] H. A. Bethe, Rev. Mod. Phys. **62**, 801 (1990).

[2] C. J. Pethick, D. G. Ravenhall, and C. P. Lorentz, Nucl. Phys. A **584**, 675 (1995).

[3] E. N. E. van Dalen, A. E. L. Dieperink, and J. A. Tjon, Phys. Rev. C **67**, 065807 (2003).

[4] P. Gögelein, E. N. E. van Dalen, C. Fuchs, and H. Müther, Phys. Rev. C **77**, 025802 (2008).

[5] I. Tanihata, Prog. Part. Nucl. Phys. **35**, 505 (1995).

[6] P. G. Hansen, A. S. Jensen, and B. Jonson, Annu. Rev. Nucl. Part. Sci. **45**, 591 (1995).

[7] M. R. Anastasio, L. S. Celenza, W. S. Pong, and C. M. Shakin, Phys. Rep. **100**, 327 (1983).

[8] C. J. Horowitz and B. D. Serot, Nucl. Phys. A **464**, 613 (1987).

[9] R. Brockmann and R. Machleidt, Phys. Rev. C **42**, 1965 (1990).

[10] E. N. E. van Dalen and H. Müther, arXiv:1004.0144 [nucl-th] (to be published in IJMPE).

[11] M. Jaminon, C. Mahaux, and P. Rochus, Phys. Rev. C **22**, 2027 (1980).

[12] M. Kleinmann, R. Fritz, H. Müther, and A. Ramos, Nucl. Phys. A **579**, 85 (1994).

[13] S. Ulrych and H. Müther, Phys. Rev. C **56**, 1788 (1997).

[14] F. de Jong and H. Lenske, Phys. Rev. C **58**, 890 (1998).

[15] D. Alonso and F. Sammarruca, Phys. Rev. C **67**, 054301 (2003).

[16] E. N. E. van Dalen, C. Fuchs, and A. Faessler, Nucl. Phys. A **744**, 227 (2004).

[17] E. N. E. van Dalen, C. Fuchs, and A. Faessler, Eur. Phys. J. A **31**, 29 (2007).

[18] W. Zuo, I. Bombaci, and U. Lombardo, Phys. Rev. C **60**, 024605 (1999).

[19] K. S. A. Hassaneen and H. Müther, Phys. Rev. C **70**, 054308 (2004).

[20] W. H. Dickhoff and H. Müther, Rep. Prog. Phys. **55**, 1947 (1992).

[21] F. de Jong and R. Malfliet, Phys. Rev. C **44**, 998 (1991).

[22] F. de Jong and H. Lenske, Phys. Rev. C **54**, 1488 (1996).

[23] R. Machleidt, Adv. Nucl. Phys. **19**, 189 (1989).

[24] H. A. Bethe, B. H. Brandow, and A. G. Petschek, Phys. Rev. **129**, 225 (1963).

[25] L. Sehn, C. Fuchs, and A. Faessler, Phys. Rev. C **56**, 216 (1997).

[26] T. Gross-Boelting, C. Fuchs, and Amand Faessler, Nucl. Phys. A **648**, 105 (1999).

[27] J. A. Tjon and S. J. Wallace, Phys. Rev. C **32**, 267 (1985).

[28] A. Trasobares, A. Polls, A. Ramos, and H. Müther, Nucl. Phys. A **640**, 471 (1998)

[29] T. Frick, K. Gad, H. Müther, and P. Czerski, Phys. Rev. C **65**, 034321 (2002).

[30] E. Schiller and H. Müther, Eur. Phys. J. A **11**, 15 (2001).

[31] E. N. E. van Dalen, C. Fuchs, and A. Faessler, Phys. Rev. Lett. **95**, 022302 (2005).

[32] E. N. E. van Dalen, C. Fuchs, and A. Faessler, Phys. Rev. C **72**, 065803 (2005).

[33] A. Ramos, A. Polls, and W. H. Dickhoff, Nucl. Phys. A **503**, 1 (1990).

[34] M. Jaminon and C. Mahaux, Phys. Rev. C **40**, 354 (1989).

[35] P. Gögelein, E. N. E. van Dalen, K. Gad, K. S. A. Hassaneen, and H. Müther, Phys. Rev. C **79**, 024308 (2009).

[36] C. Mahaux, P. F. Bortignon, R. A. Broglia, and C. H. Dasso, Phys. Rep. **120**, 1 (1985).